

Simulations for Multi-Object Spectrograph Planet Surveys

Stephen R. Kane¹, Donald P. Schneider², Jian Ge¹

¹*Department of Astronomy, University of Florida, 211 Bryant Space Science Center, Gainesville, FL 32611-2055, USA*

²*Department of Astronomy and Astrophysics, Pennsylvania State University, 525 Davey Laboratory, University Park, PA 16802, USA*

10 June 2021

ABSTRACT

Radial velocity surveys for extra-solar planets generally require substantial amounts of large telescope time in order to monitor a sufficient number of stars. Two of the aspects which can limit such surveys are the single-object capabilities of the spectrograph, and an inefficient observing strategy for a given observing window. In addition, the detection rate of extra-solar planets using the radial velocity method has thus far been relatively linear with time. With the development of various multi-object Doppler survey instruments, there is growing potential to dramatically increase the detection rate using the Doppler method. Several of these instruments have already begun usage in large scale surveys for extra-solar planets, such as FLAMES on the VLT and Keck ET on the Sloan 2.5m wide-field telescope.

In order to plan an effective observing strategy for such a program, one must examine the expected results based on a given observing window and target selection. We present simulations of the expected results from a generic multi-object survey based on calculated noise models and sensitivity for the instrument and the known distribution of exoplanetary system parameters. We have developed code for automatically sifting and fitting the planet candidates produced by the survey to allow for fast follow-up observations to be conducted. The techniques presented here may be applied to a wide range of multi-object planet surveys.

Key words: methods: data analysis – planetary systems – techniques: radial velocities

1 INTRODUCTION

Of all the methods used for the detection of extra-solar planets, the radial velocity (or Doppler) technique is still the dominant source of extra-solar planet discoveries. There are currently more than 15 independent groups searching for exoplanets using the Doppler method, most notably the California & Carnegie Planet Search (Marcy et al. 1996) and the High Accuracy Radial velocity Planet Searcher (HARPS) (Pepe et al. 2004) teams, whose combined efforts have led to the majority of exoplanet discoveries thus far. A number of advancements in the radial velocity technique have gradually increased the rate of exoplanet discoveries. Improvements to single-object spectrograph design have resulted in a number of the groups obtaining measurement accuracies close to the current practical limit for ground-based radial velocity searches of $\sim 1 \text{ m s}^{-1}$. The strategy adopted by many of the groups is to use increasingly larger telescopes which dramatically increases (normally by at least an order of magnitude) the number of stars which are accessible to the particular survey. Also, a few of the groups have now been monitoring stars for a lengthy period of time such that they are able to detect planets with orbits larger than 5 AU.

The majority of current radial velocity surveys make use of very high resolution echelle spectrographs (Butler et al. 1996) and rely on measurements of the shift relative to a reference spectrum, either by cross-correlation or fits to line profiles. However, as well as being expensive, these instruments can suffer from low throughput and can only observe a single object in each observation. A solution to this problem is to utilise fibre-fed multi-object instruments, such as the FLAMES instrument on the VLT (Pasquini et al. 2002). The relatively small field-of-view (FOV) in this case is compensated by the large magnitude depth which is able to be probed, and FLAMES has already been used to confirm several transiting planet candidates (Bouchy et al. 2004). Another example is Hectochelle (Szentgyorgyi et al. 1998); a high-resolution, multi-object instrument in operation on the 6.7m MMT which, though there are currently no plans to do so, has the potential to perform an extensive survey for extra-solar planets. Multi-object spectrographs such as these have the potential to increase the survey volume by many orders of magnitude and thus would have an enormous impact on the discovery rate of exoplanets using the Doppler method.

The multi-object instrument proposed by Ge (2002) is of a particularly unique design which does not utilise an echelle spectrograph. A prototype of the instrument, called Exoplanet Tracker (ET), was used by van Eyken et al. (2004) to detect the radial velocity signature of the planet orbiting 51 Peg. The Exoplanet Tracker is a fibre-fed dispersed fixed-delay interferometer, which is essentially a combination of a Michelson interferometer and medium resolution spectrograph. This instrument allows the simultaneous observing of multiple targets, is relatively cheap to build, and the lower resolution allows for a much higher throughput, thus increasing the effective magnitude depth of the survey. The first planet discovered using ET (Ge et al. 2006) demonstrated the successful application of the interferometer design. Based on the early successes of the ET instrument using the 0.9m Coudé and 2.1m telescopes at KPNO, an upgraded multi-object version of the dispersed fixed-delay interferometer, named the Keck ET, was designed for testing on the Sloan Digital Sky Survey 2.5m telescope (Gunn et al. 2006) at Apache Point Observatory, New Mexico. Engineering tests of the Keck ET were performed in 2005, and the first science-quality data were obtained during commissioning in the spring and summer of 2006.

To support the variety of multi-object planetary search programs, we have undertaken an extensive coding effort to produce simulations to guide the observational programs. This study was originally motivated by the need to produce accurate simulations of the data quantity and quality for surveys based upon the observing time and target list, hence predicting the expected planet yield. This study also provide estimates of the number of measurements required for a significant detection and methods for reducing the number of false detections due to noise mimicing period signals.

We present the methods and results of the simulations for multi-object planet surveys. Section 2 gives a brief overview the development and architecture of the simulation/fitting code. Section 3 describes the method used to generate the simulated data including assumed planet distribution/parameters and noise models. Section 4 explains the methods used for sifting the data for planet candidates and fitting models to the data. Section 5 describes the expected results from a given survey, how these results depend upon the observing window and period distribution, and the number of planets one can expect to transit their parent star. Section 6 presents an analysis of the number of stars available as suitable candidates for a variety of fields and magnitude depths. Section 7 discusses various possible improvements to the simulations, the application to target selection, and stellar metallicity considerations. Finally, it is shown how these methods and results may be applied to a wide variety of surveys for extra-solar planets.

2 SCIENTIFIC RATIONALE FOR MULTI-OBJECT SURVEYS

There are currently more than 200 known extra-solar planets. These planets have revealed a broad range of possible exoplanetary orbital and physical parameters which have challenged and subsequently resulted in the revision of theories regarding planet formation. For example, the migration of planets into short-period orbits has been explained via inter-

actions with the protostellar disk (Lin et al. 1996) and other planets (Rasio & Ford 1996). Also, the excitation of planets into highly eccentric orbits has been explained through such processes as resonant interactions (Lee & Peale 2002) and secular interactions (Adams & Laughlin 2006) with other planets. This great diversity in planet parameters requires a large number of new discoveries which can provide statistically meaningful ways of understanding their origins.

Although the high-precision echelle radial velocity instruments have been quite successful in detecting extra-solar planets, the detection rate has thus far proceeded in an almost linear fashion due to the limitations of the echelle techniques being used. These limitations include such aspects as the costly approach of requiring large amounts of large telescope time and the sinlge-object capability of the instruments, but can also include other factors such as a relatively low throughput. In addition, many surveys have limited their target selection to stars brighter than a visual magnitude of ~ 8.0 ; an exception being the N2K survey which probes stars brighter than ~ 10.5 (Fischer et al. 2005). These current echelle techniques limit the number of new planet discoveries possible in the near future and so limit the information available to provide refinements to planetary formation theories.

The large number statistics required to study the observed diversity amongst exoplanets can be addressed via multi-object surveys which have the potential to increase the detection rate by at least an order of magnitude. An advantage of this method is that it removes the need to search only high-metallicity stars to increase the probability of planet detection (Fischer & Valenti 2005) and can therefore yield an unbiased sample of the stellar properties of the sample stars. This will allow for a more complete study of correlations between planet frequency with a variety of spectral parameters. Furthermore, the distribution of planet parameters, such as the mass distribution, will be constrained to much higher accuracy and additional challenges to current planet formation theories possibly revealed. A valuable bonus aspect of such a survey will be to provide accurate absolute radial velocities for many thousands of stars, vastly increasing our knowledge of stellar and galactic kinematics in the solar neighbourhood.

The importance of transiting giant planets to understanding planet formation is enormous since they are the only exoplanets for which we can determine both masses and radii. The planetary mass-radius relation is slowly developing our knowledge of planetary structure and evolution, analogous to the stellar mass-radius relation for stars. It is likely that a large, multi-object survey such as the type described here will yield many transiting exoplanets through efficient photometric follow-up of the radial velocity discoveries. These additional transiting planets will prove invaluable to understanding the dependence of planetary radius on the mass, age, and the composition of both the core and the gaseous envelopes of giant planets. Further observations of these planets using Spitzer, such as those undertaken by Deming et al. (2006), will lead to refined planetary atmosphere models which can describe in detail the efficiency of heat transport from the dayside to the nightside of hot Jupiters subject to large amounts of stellar irradiation.

3 RADIAL VELOCITY SIMULATION CODE

Simulations for the expected planet yield play an important role in the development of extra-solar planet surveys. There are numerous examples of this for the transit method, such as the planet yield simulations performed by Horne (2003) for a variety of transit surveys and those performed specifically for the Kepler mission by Borucki et al. (2003). An exhaustive FORTRAN code for simulating transits due to exoplanets and the expected planet yield called `transim` (Transit Simulator) was developed and then applied to the WASP0 instrument (Kane et al. 2005). A similar FORTRAN code, a few aspects of which are described in this paper, has been developed for application to radial velocity exoplanet surveys, called `rvsim` (Radial Velocity Simulator).

The primary purpose of both `transim` and `rvsim` is to allow the user to work with both simulated and real data simultaneously to allow accurate comparisons to be made between them, and to produce all the fits and statistical analysis for the data. For example, the `transim` code includes a transit detection algorithm for sifting planet candidates from the vast amount of photometric data. The `rvsim` code also includes sifting and fitting routines which will be described in detail in later sections. Since the observing and instrument parameters are fully customisable, the code is perfectly able to adapt to almost any planned survey. The code was extensively tested using realistic simulations of large-scale planet surveys. A few of the main capabilities of `rvsim` are demonstrated in this paper.

4 SIMULATED DATA

To estimate how many planets we expect to detect in a given radial velocity observing program, we performed a series of Monte-Carlo simulations which inject planets into a realistic sample of target stars based on the known distribution and characteristics of exoplanets. This section describes the generation of the simulated data.

4.1 Besançon Models

A realistic stellar population from which to generate our synthetic data may be obtained via the Besançon Galactic model (Robin et al. 2003). This model is able to derive observational predictions from an overall description of Galactic structure and evolution, where the model includes four populations (thin disc, thick disc, spheroid, bulge). Hence, one can simulate the Galactic stellar populations in any directions in a wide-range of photometric bands. The resulting model produces a catalogue of pseudo-stars for a given field from Monte-Carlo simulations of the model. The accompanying stellar parameters are then ideal for evaluating the feasibility of observing particular fields.

For the purposes of the simulation presented in this paper, a stellar population model was calculated for a magnitude limited survey in the Kepler field. According to Jenkins et al. (2005), this field covers ~ 105 square degrees and is centered on Galactic coordinates $l = 76.3^\circ; b = 13.5^\circ$. Jenkins et al. (2005) used a Besançon model to estimate that the relocation of the Kepler field slightly decreases

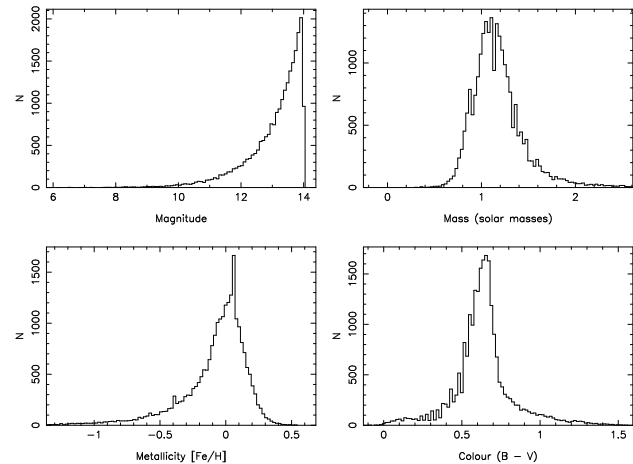


Figure 1. Properties of stars included in the simulation sample, as derived from the Besançon model. Distributions include the magnitude (top-left), the stellar masses (top-right), the metallicities (bottom-left), and the $B - V$ colours (bottom-right).

the number of primary target stars, but dramatically reduces contamination due to false positive planet detections. Mahadevan et al. (2005) noted that the Kepler field is an ideal location for a multi-object radial velocity survey since the results would not only compliment the transit survey to be undertaken by the Kepler mission, but also aid in target selection.

A Besançon model tailored to the Kepler field for $6.0 < m_V < 14.0$ created a distribution of magnitudes, colours, and metallicities from which stellar parameters were derived. Stellar radii for main sequence stars were calculated directly from the colours provided and giant stars were excluded from the analysis. This created a sample of 75195 stars from which 51487 giant stars were excluded, leaving 23708 main sequence stars. Figure 1 shows the histograms of the resulting sample of stars used for the simulations. The stellar population in the Kepler field is largely comprised of main sequence stars with mostly solar metallicity.

4.2 Planet Distribution

The distribution of planets amongst main sequence stars has gradually emerged over recent years. Several thousand nearby solar-type stars have been monitored by radial velocity surveys, from which it has been found that at least 5% of these stars harbour an extra-solar planet (Lineweaver & Grether 2003). Moreover, approximately 11% of stars which have been monitored for more than 15 years harbour a planet and 0.5%–1% of solar-type stars in the solar neighbourhood have been found to harbour a Jupiter-mass companion in a 0.05 AU (3–5 day) orbit. Marcy et al. (2005) note that at least 6.6% of their survey stars harbour a planet with a mass less than 13 Jupiter masses and with a semi-major axis within 5 AU. However, they also note that they are restricted to M dwarfs within 10 pc due to their faintness, thus our knowledge of the planet distribution around late-type stars is less well known.

In order to be even more quantitative regarding the planet distribution, we can utilise the planet-metallicity correlation presented in Fischer & Valenti (2005) which relates

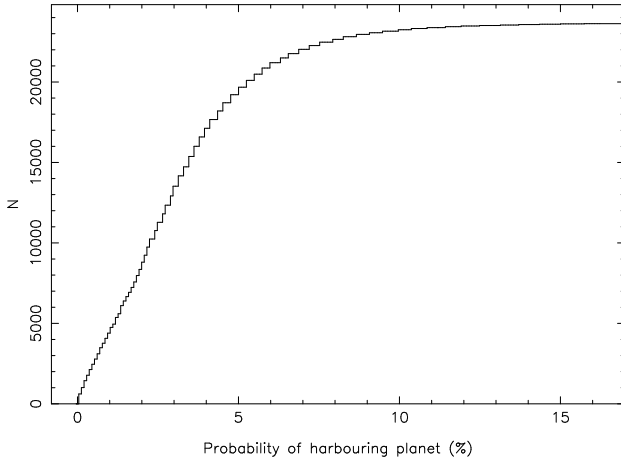


Figure 2. Cumulative histogram of the probability of harbouring a planet for all the stars in the sample based upon the metallicity.

stellar metallicity to planetary abundance. For each of the stars in the simulation, the probability of each star harbouring a planet was computed based on the metallicity provided by the Besançon model. Figure 2 shows a cumulative histogram of the planet-harbouring probability for the sample, which demonstrates the substantial reduction in planet-harbouring stars beyond a probability of around 5%. As can be seen from Figure 1, the stellar population in the Kepler field is largely comprised of main sequence stars with mostly solar metallicity. The power law nature of the Fischer & Valenti (2005) correlation tends to dramatically increase the number of stars with low planet-harbouring probability for a typical metallicity distribution. In particular, stars with metallicities less than ~ -0.5 dex were found to have essentially zero probability of harbouring a planet.

For the 23708 stars in this sample, a Monte-Carlo simulation of the planet-harbouring probability yielded a result of 751 planet-harbouring stars in the sample. Prior to this, tests were performed which assumed that 90% of stars have planets. This initial simulation was used as a successful test of the `rvsim` code to detect planets in the data and extract the correct planet parameters.

4.3 Radial Velocity Calculations

Detecting a companion to a star using the Doppler technique relies on being able to measure a periodic change in the radial component of the stellar velocity. The measured radial velocity, V , is given by

$$V = V_0 + K(\cos(\omega + f) + e \cos \omega) \quad (1)$$

where V_0 is the systemic velocity, K is semi-amplitude, ω is the argument of periastron, f is the true anomaly, and e is the eccentricity. The true anomaly, f , is the angle between the position at periastron and the current position in the orbit measured at the focus of the ellipse. The true anomaly can be expressed as $f = f(t, t_0, e)$ where t_0 is the time at periastron. The semi-amplitude of the radial velocity, K , may be further expressed as

$$K = \left(\frac{2\pi G}{P} \right)^{1/3} \frac{M_p \sin i}{(M_* + M_p)^{2/3}} \frac{1}{\sqrt{1 - e^2}} \quad (2)$$

where P is the period, i is the inclination of the planetary orbit, and M_p and M_* are the masses of the planet and parent star respectively. The period is also related to the semi-major axis of the planetary orbit via Kepler's third law:

$$P^2 = \frac{4\pi^2 a^3}{G(M_* + M_p)} \quad (3)$$

Equation (1) gives the radial velocity as a function of the true anomaly, f . To calculate the radial velocity as a function of time it is necessary to find f as a function of t . The mean anomaly is defined as

$$M = \frac{2\pi}{P}(t - t_0) \quad (4)$$

and is hence the fraction of the orbital period that has elapsed since the last passage at periastron. From the mean anomaly we can calculate the eccentric anomaly, E , which is the angle between the position at periastron and the current position in the orbit, projected onto the ellipse's circumscribing circle perpendicularly to the major axis, measured at the centre of the ellipse. These two quantities are related via Kepler's equation:

$$M = E - e \sin E \quad (5)$$

which has the solution

$$E = \frac{M - e(E \cos E - \sin E)}{1 - e \cos E} \quad (6)$$

This can be solved via a Newton-Raphson iteration which converges when $|(E_{\text{new}} - E_{\text{old}})/E_{\text{old}}|$ is less than some sufficiently small number. The radial velocity code in `rvsim` chooses this convergence value to be 10^{-4} . In addition to this, Charles & Tatum (1998) have shown that this iteration will always converge if the initial guess of the elliptical anomaly is chosen to be $E = \pi$. This method rapidly yields the value of E (usually in only a few iterations) and hence the value of f :

$$\cos f = \frac{\cos E - e}{1 - e \cos E} \quad (7)$$

Equation (1) can now be evaluated as a function of time.

Combining these calculations with a χ^2 analysis results in a fitted radial velocity curve from which it is possible to determine the values of P , V_0 , K , ω , t_0 , and e . The calculations are relatively computationally inexpensive and so can be performed on a large number of datasets in a reasonably short period of time. This is an important factor in the methods used to search parameter space discussed in later sections.

4.4 Planet Parameters

Over 180 planets are now known via the various radial velocity surveys. The number of planet discoveries and the duration of the surveys has now allowed a more complete picture of exoplanetary parameter space. Understanding the distribution of these exoplanetary parameters is critical to creating an accurate simulation of the expected planet yield from a survey since this will determine which planets the experiment is sensitive enough to detect.

As discussed earlier, each star in the simulation was assigned a planet-harbouring probability based on the metallicity. This information provided the basis of a Monte-Carlo

simulation which showed that one could generally expect 751 stars in the sample to harbour planets. For the purposes of demonstrating the expected exoplanetary parameter distribution, we have assumed that each planet-harbouring star has only one planet. Each planet was then assigned parameters in a process repeated many times via an additional Monte-Carlo simulation. The range of distribution of these parameters were drawn from a variety of sources, including The Extrasolar Planets Encyclopaedia¹. In addition, more precise estimates of planetary parameters have been recently published by Butler et al. (2006). This process used here to select planet parameters will now be described in more detail.

The first parameter to be assigned was the planetary mass. The exoplanetary mass function has most recently been determined to be roughly described as

$$\frac{dN}{dM_p} \sim M_p^{-1.05} \quad (8)$$

by Marcy et al. (2005). It has been noted by Jorissen et al. (2001) and Zucker & Mazeh (2001) that this mass distribution is largely unaffected by the unknown $\sin i$ component. The inclination of the planetary orbit is chosen to randomly lie between 0° and 90° . The discovery of a sub-Neptune mass by Beaulieu et al. (2006) implies that this mass distribution is likely to continue into the regime of rocky planets, suggesting that terrestrial planets may be common. By choosing a lower and upper mass limit of 0.02 and 13.0 Jupiter masses respectively, this mass function was used to randomly determine the planet masses. It should be noted that this does not take into account possible variation in planet mass with host mass such as, for example, that suggested by Adams et al. (2006). Also neglected is the apparent rise in mass with stellar host metallicity (Fischer & Valenti 2005).

The second parameter to be assigned was the period of the planetary orbit. Based on the work of Tabachnik & Tremaine (2002), a good approximation of the period distribution is to assume that exoplanetary periods are uniform in log space. The upper and lower limits for the period distribution were chosen to be 1 and 2000 days respectively, which is equivalent to 0.02 to ~ 3 AU for a solar-type stellar host. These limits encompass the majority of the currently known exoplanets and allows for surveys durations which extend slightly beyond 5 years. However, the smooth logarithmic function which is assumed for this simulation does not take into account the apparent ‘‘period valley’’ which exists between 10 and 100 days, as noted by Udry et al. (2003). There is an apparent ‘‘pileup’’ of planetary periods which occurs near 3 days, as clearly shown by Butler et al. (2006). This is accounted for in the code by suppressing periods of less than 3 days duration to produce an identical period distribution to that seen amongst real exoplanets.

The source of the eccentricity of extra-solar planets is generally not well understood, particularly with regards to planet formation. Exoplanets have been found to possess a wide range of eccentricities, mostly between 0.0 and 0.8 (Marcy et al. 2005). These eccentricities appear to be mostly random with a gradual increase in the eccentricity upper

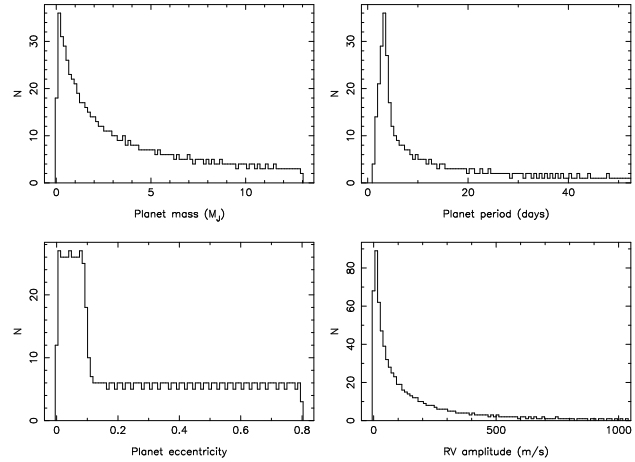


Figure 3. Results of a Monte-Carlo simulation of the expected distribution of planet parameters. Distributions include the planet mass (top-left), the planet period (top-right), the planet eccentricity (bottom-left), and the radial velocity amplitude of the parent star due to the planet (bottom-right).

limit with increasing semi-major axis. The exception is planets with a semi-major axis less than 0.1 AU, where the orbits have been forced into nearly circular orbits due to tidal circularization. Therefore for this simulation the eccentricity distribution was approximated by allowing it to be randomly selected between 0.0 and 0.8. For those orbits inside of 0.1 AU, the eccentricity was randomly selected between 0.0 and 0.1.

With the simulated planet parameters described above, the amplitude of the induced radial velocity was calculated for each star using equation (2). This process of parameter simulation and radial velocity calculation was repeated many times through a Monte-carlo simulation, the results of which are shown in Figure 3. Based on the radial velocity amplitude histogram, the number of expected planet detection can then be estimated based on the precision of the experiment.

4.5 Noise Model and Error Sources

To approximate error bars for the simulated radial velocity data, one must consider the various sources of noise associated with the data. The standard noise model takes into account detector characteristics as well as photon statistics and takes the form

$$\sigma^2 = \sigma_0^2 + \frac{(f_* + f_{\text{sky}})\Delta t}{G} \quad (9)$$

where σ_0 and G are the CCD readout noise (ADU) and gain (e^-/ADU) respectively, f_* and f_{sky} are the star and sky fluxes respectively, and Δt is the exposure time. For the purposes of this particular application, it is sufficient to consider the various components of equation (9) individually and then combine them together.

There are three components which contribute to the error in the observed radial velocity. The first is the photon noise, σ_p which is approximated as a simple scaling law

$$\sigma_p = \sqrt{100^{(m_V - 8.0)/5}} \times \sigma_{8.0} \quad (10)$$

¹ <http://exoplanet.eu/>

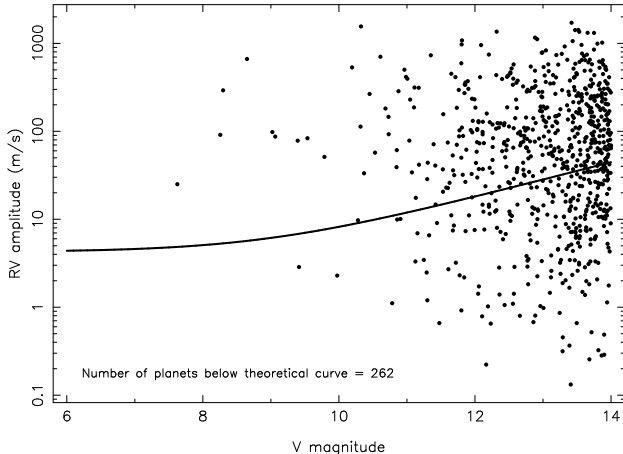


Figure 4. A radial velocity amplitude vs magnitude diagram for the simulated planets, showing the theoretical accuracy curve based on the noise model of the experiment.

where $\sigma_{8.0}$ is the rms photon noise at a V magnitude of 8.0. The photon noise is generally the most important of the sources of error since it effectively defines the depth of the survey. For this simulation, we adopt a value of $\sigma_{8.0} = 2.8 \text{ m s}^{-1}$ for a one hour exposure based on typical photon noise estimates from various surveys, studies performed by Bouchy et al. (2001), and estimates provided by Ge et al. (2006).

The second component is the noise contribution due to systematic errors, σ_s . Noise contributions due to systematic errors are often the most frustrating component since they can originate from a wide range of sources including the hardware and the data reduction software. These include imperfections in the grating, biases inherent in the CCD detector, flat-fielding, and moon illumination. A multi-object instrument may have additional sources of systematic errors such as cross-contamination between spectra, aberration/distortion of the spectra near the edge of the detector, and guiding errors from tracking multiple stars. Based on conservative estimates from these various noise sources, a systematic rms error of $\sigma_s = 3.0 \text{ m s}^{-1}$ is assumed for this simulation.

This third source of errors considered here is that resulting from stellar intrinsic variability caused by chromospheric activity, denoted as σ_i . The causes of stellar intrinsic radial velocity noise has been described in great detail in the literature, for example by Saar et al. (1998) and Saar & Fischer (2000). The recent revision of planet parameters by Butler et al. (2006) allowed a more robust quantitative estimate of this “jitter” noise by employing the methods described in Wright (2005). We account for the intrinsic variability of our simulated stars by adopting $\sigma_i = 3.0 \text{ m s}^{-1}$, which is the estimated median jitter for G and K dwarfs. It should be noted that this does not include stellar seismic activity (p-modes) Dall et al. (2006). This activity is well illustrated by the study of the μ Arae system (Santos et al. 2004; Bouchy et al. 2005). The high frequency of seismic activity often means that it only significantly effects observing programs which use a relatively short exposure time, such as HARPS (Mosser et al. 2005).

The three components are then added in quadrature to obtain the total rms error per star:

$$\sigma^2 = \sigma_p^2 + \sigma_s^2 + \sigma_i^2 \quad (11)$$

Figure 4 shows a typical distribution of the radial velocity amplitude of simulated planets over the full magnitude range. Also shown is the theoretical accuracy curve (equivalent to the 1σ threshold using the above formula); the number of planets that fall below this curve are therefore unlikely to be detected with the current experiment.

This simple model is not without limitations but is more than sufficient for the simulation presented here. For example, purely photon noise scaling is just indicative for fainter stars and it is likely that a systematic noise threshold is reached for lower fluxes. In addition, the intrinsic stellar variability does vary with spectral type and luminosity class, particularly for M dwarfs and subgiants, which means the jitter will be underestimated slightly in some cases. The simulations presented here only include a single planet for each planet-harbouring star, whereas there are likely to be additional planets in longer period orbits whose low amplitude signal will initially contribute to the jitter noise. Further observations will extract the periodic nature of these signals once there has been sufficient phase coverage of the planetary orbit. Spectroscopic binary stars are highly likely to be present in the real planet survey data but are not considered here since they are easily detected and readily distinguishable from planetary candidates.

4.6 Radial Velocity Precision and Planet Detectability

An important quantity to determine from the simulation is the number of planets detectable for a given instrument precision. Recall that from the Besançon model of 23708 stars, a Monte-Carlo simulation of the planet-harbouring probability showed that ~ 750 of those stars would harbour a planet. The distribution of known planet parameters was then used to calculate the expected distribution of radial velocity amplitudes for those stars. This information can then be used to determine approximately the number of planets one can detect as a function of the rms radial velocity precision of the instrument, assuming that the precision includes noise from all sources.

Figure 5 shows the number of planets detectable from the simulated data at the 3σ level as a function of the rms radial velocity precision. The range of precision values shown was chosen to encompass a broad range of radial velocity experiments. As shown in the figure, for a radial velocity precision of 10 m s^{-1} , one may expect to detect ~ 520 of the planets in the simulated sample. Likewise, for a radial velocity precision of 5 m s^{-1} , one may expect to detect ~ 601 of the simulated planets. In this example, doubling the precision of the instrument (from 10 m s^{-1} to 5 m s^{-1}) only increases the planet yield by $\sim 15\%$. In general, doubling the number of survey stars will obviously increase the planet yield by 100%. Thus, the design of the experiment will depend upon whether one aims to increase mass sensitivity or increase overall planet sensitivity, since improving the radial velocity precision is not nearly as important as increasing the number of survey stars for increasing the net planet yield. This demonstrates the power of new multi-object planet surveys

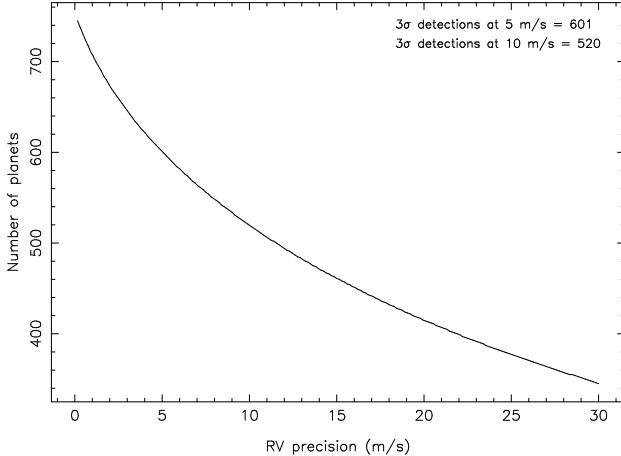


Figure 5. The number of planets detectable at the 3σ level from the simulation sample as a function of the rms radial velocity precision of the experiment.

for dramatically increasing the number over known exoplanets over a relatively short period of time. However, this calculation does not take into account that an improved radial velocity precision would allow fainter stars to be available for follow-up observations, assuming that the experimental accuracy is photon-limited. Another important point is that this calculation only takes into account single measurements, whereas multiple measurements will of course improve the rms precision at which one is able to detect signatures of a given amplitude. In particular, folding the data over multiple periods will significantly increase the power of the planetary signal and therefore improve the detectability of the planet. This is true for both single and multiple object surveys.

4.7 Observing Window and Interruptions

The duration of the observing window is of key importance since it determines the orbital periods to which one is sensitive from initial observations of the targets. For the simulated data, an observing window of 30 days was assumed which allows a broad range of tests to be performed which can be scaled to the size of the real observing window. It is also assumed that a single observation is obtained per star per night. These times of observations were passed through a gaussian filter, depending upon the number of observations per night per star, which ensured that each star was not observed at exactly the same time each night.

However, any observing run is subject to the unpredictable nature of the weather. This is taken into account by specifying the fractional number of clear nights for a given observing site. For each simulated star, it is randomly determined per night if data was acquired on that target. For this simulation, we have assumed that 60% of the nights are available for spectroscopic observations, which is typical for most observatories.

5 RADIAL VELOCITY FITTING

In this section we describe the method used for automatically sifting planet candidates from the data and the iterative grid-search technique used to fit models to those candidates.

We also discuss the false-alarm rate and the dependence of successful detections upon various star and planet parameters.

5.1 Sifting the Data

The formidable task that remains once the data has been acquired and processed is to efficiently extract planet candidates from the dataset. This is particularly important for large-scale surveys, transiting planet surveys for example, in which a relatively automated method must be constructed in order to (a) keep the data analysis rate at a level which is at least as fast as the data acquisition rate, and (b) to prevent missed detections since sifting the data manually will not always be able to discern a periodic signature unless phase-folded. The `rvsim` code will ingest either real or simulated data and attempt to perform such a sifting operation by making use of data statistics combined with a weighted Lomb-Scargle fourier period analysis.

For the period analysis, we make use of the Lomb-Scargle (hereafter L-S) periodogram method (Lomb 1976; Scargle 1982) which is especially suited to unevenly sampled data. This method, which uses the Nyquist frequency to perform spectral analysis of the data, produces a “L-S statistic”, which is the fourier power calculated at each frequency over a range of frequencies. The maximum fourier power is the frequency which yields the least squares fit of a sinusoidal model to the data. The L-S statistic also indicates the significance level of the fit at that particular frequency and hence reveals the likely value for the period. If one scans over M independent frequencies, then for a fourier power $P(f)$ at frequency f , the probability P that other frequencies in the scanned region have a higher power is

$$P(> P(f)) = 1 - (1 - e^{-P(f)})^M \quad (12)$$

which is also referred to as the false-alarm probability. For example, a probability of 0.1 indicates that the peak in question has a 10% chance of being due to a false-alarm and thus we are 90% confident in the significance of the peak at that frequency. Figure 6 displays an example periodogram for one of the simulated stars. The dotted lines show the false-alarm probabilities from 50% to 0.1%.

An issue which can arise when using the standard L-S periodogram is the fact that experimental uncertainties are neglected entirely in the calculation of the fourier power. The standard L-S is inversely proportional to the variance of the entire dataset which is completely independent of the individual variances on each data point. In general, the standard L-S provides a robust period analysis assuming that the error bars are reasonably similar such as data acquired from the same instrument. In cases where one wishes to combine data from several sources which may have substantially different uncertainties, a more complete period analysis can be achieved by appropriately weighting the fourier power calculation. An example of this can be seen in Ge et al. (2006) where radial velocity data from KPNO was combined with follow-up data from the HET.

A weighted L-S period analysis for `rvsim` was created using the methodology shown in Aharmin et al. (2005). This method applies inverse variance weighting calculated for each data point to each of the terms in the fourier component. In cases where the error bars (and hence the weights)

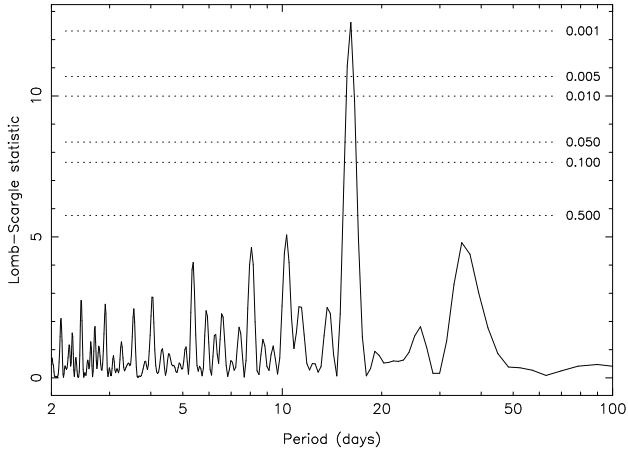


Figure 6. An example L-S periodogram for a simulated star which harbours a planet. The dotted lines indicate the probability that the fourier power is a false-alarm and hence the confidence one can have in the period.

are equal, the weighted L-S periodogram reduces to the standard L-S periodogram.

The first step of the automated fitting routines of `rvsim` is to subject each dataset to a number of statistical tests that categorise the star based on the outcome of the tests. The first test is a weighted L-S period analysis which attempts to detect a periodic signature in the data. If a frequency is found for which the false-alarm probability is less than a user specified value, 50% for example, then the data is classified as “periodic” and is passed to a fitting code (described later) for more thorough analysis. It should be noted that periods of less than ~ 1 day are assumed to be aliases and are discarded in favour of the next highest fourier peak. This not only leads to a more accurate period estimation but also dramatically decreases the rate of false detections.

If, on the other hand, no periodic signal is detected then a variability statistic based on the rms scatter and standard deviation of the data is used flag those stars for which there is sufficient variability. These stars are classified as “variable” and are noted for future investigations since planets with periods substantially longer than the observing window are unlikely to show a periodic signature until more phase coverage is achieved. If a star fails to be classified as either periodic or variable then it is classified as “unknown”, which means it is presumed to be a constant star at least until further data can be acquired. As shown in the following sections, this technique is an effective method for recovering planetary signatures in radial velocity data down to the photon noise-limit of the instrument.

5.2 Detection Efficiency and False-Alarm Rate

The efficiency of this method for detecting real planetary signatures in the data and its frequency of false detections is dependant upon a number of factors. The most obvious and dominant factor is the false-alarm probability threshold which one chooses to classify data as being periodic. As the probability threshold is increased, the number of successful planet detections will increase but the number of false detections will also increase. Although one seeks to keep the number of missed planetary detections to a minimum, the issue

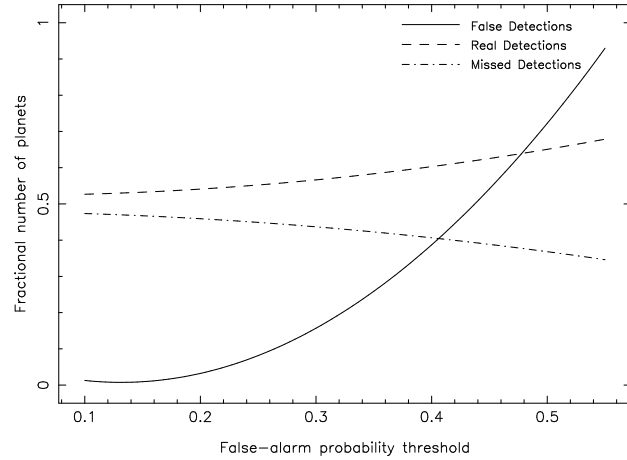


Figure 7. Dependence of false, real, and missed detections on the chosen periodic false-alarm probability threshold.

of false detections can become serious if the required follow-up observations begin to substantially compromise the total observing time of the experiment and thus compromise the overall planet yield.

In order to determine exactly how these detections depend upon the false-alarm probability threshold, the method was tested using a specific dataset and a range of probability threshold values. Shown in Figure 7 is the resulting relation on the probability threshold for false detections, real detections, and missed detections. The figure shows that the number of false detections is sensitively dependant on the false-alarm probability threshold, whereas the number of real detections is relatively independent of the cutoff. If one chooses to restrict the periodic signatures to those which pass a 10% probability threshold, one will have eliminated essentially all of the false detections without severely compromising the total planet yield.

The range of real detection rates varies from around 55% at a probability threshold of 10%, to around 65% at a probability threshold of 50%. Considering that these numbers already take into account those planets which fall below the theoretical accuracy curve discussed earlier, these numbers may seem to indicate a quite low detection level. However, two further factors which affect the number of detections from the data are the number of data points acquired per target, and the period of the planetary orbit relative to the observing window of the observations.

To provide quantitative estimates on how these factors effect the detection rates, we performed several experiments using a simulated dataset in which all of the stars are assumed to have planets and there are no interruptions due to weather. This simulation was created to provide the most accurate statistics since we are only interested in the number of successful detections, not false detections, for these tests. A L-S periodogram analysis was performed on each star’s observations, and only those stars which satisfied the following criteria were selected: (1) the probability of the periodic signal being a false-alarm is less than 10% and (2) the initial period estimate from the periodogram is within 10% of the true period. For each selected star the number of data points and the period as a fraction of the observing

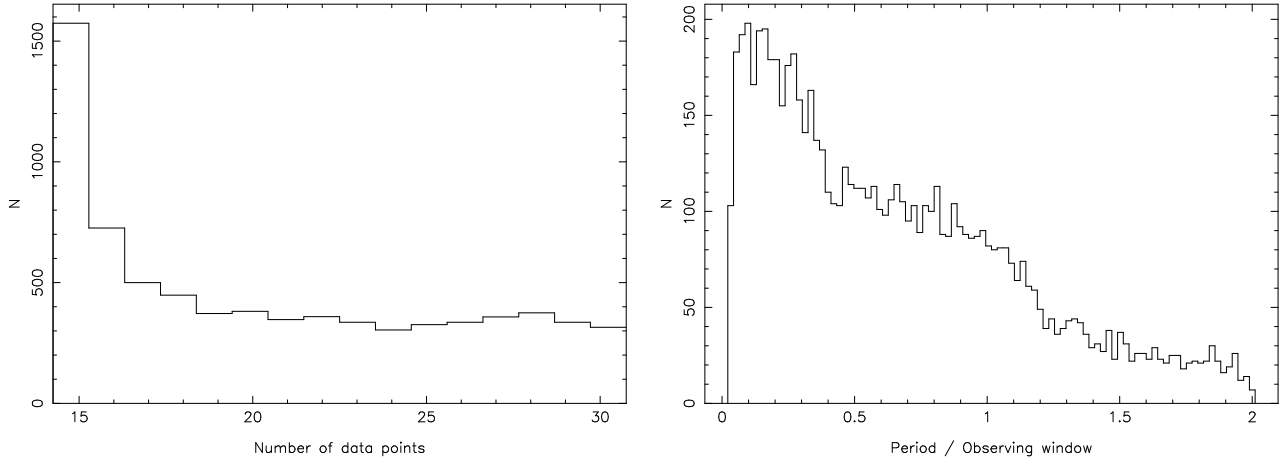


Figure 8. Histograms based on tests performed to determine the dependence of successful detections on the number of data points (left) and the planetary period (right).

window were determined. Recall that the observing window for the simulated data is 30 days.

The resulting histograms are shown in Figure 8. The histogram of the number of data points required for selection shows that the majority of stars need ~ 15 data points to pass the test. The scatter in the data shown in the histogram is a combination of two factors: (a) photon statistics dominating at faint magnitudes and thus increasing the number of data points required for a successful detection, and (b) periods longer than the observing window not having sufficient period coverage to secure a detection. The second histogram investigates the dependence of period (or phase) coverage on the number of successful detections by expressing the period as a fractional duration of the observing window. The histogram clearly shows an approximately linear dependence with the number of datasets passing the test dropping to almost zero once the period of the planetary orbit exceeds twice the length of the observing window. This is a selection effect one would expect for detecting planets with periods smaller than the observing window. However, it helps one to understand the effect this factor has on the overall planet yield from a duration limited survey when expressed in this fashion.

5.3 The Fitting Algorithm

There are many methods one can select when attempting to model astronomical data, such as bayesian techniques, genetic algorithms, and simulated annealing. Since the aim of this fitting algorithm is to provide a reasonably robust fit in an automated fashion to a multitude of data, the method that was used for this analysis is an iterative grid-search approach. The method is similar in many respects to the amoeba, or downhill-simplex method, and proves to be remarkably robust against falling victim to local minima. The iterative grid-search method is described in more detail below.

The first step of the fitting process is to estimate a range values for each fit parameters over which to conduct the search. Most of the initial guesses of the fit parameters do not assume a priori knowledge per se, but rather rely on

the period provided by the L-S periodogram and the overall statistics of the data itself. There are six parameters which are independently fit: the period P , the systemic velocity V_0 , the semi-amplitude K , the argument of periastron ω , the time at periastron t_0 , and the eccentricity e . The fitting of the argument of periastron and the eccentricity do use the a priori knowledge that they are limited by $0 < \omega < 2\pi$ and $0 < e < 1$ respectively.

After the minimum and maximum values for each of the fit parameters have been established, a grid is constructed by dividing the range of values for each parameter into equal segments. The number of segments the grid is divided into depends upon the grid precision g_p which is defined by the user. The function (in this case, the radial velocity model described in section 3.3) is then evaluated at g_p+1 points on the grid for each parameter including the current minimum and maximum values. The points on the grid which produce the minimum χ^2 are then used as the central values for the next iteration which uses the grid precision to new minimum and maximum values over which to search. This process is repeated until either the improvement in χ^2 is less than 10^{-3} or the number of iterations exceeds 15. The method is able to provide excellent fits to almost all of the planetary data with little or no human interaction.

Shown in Figure 9 are some typical examples of simulated radial velocity data for stars harbouring a planet and the best-fit models. These fits only used a grid precision of 6 and so covered on the solution quite rapidly. The data have a range of parameter values, particularly the period and the eccentricity. Since the eccentricity defines the shape of the radial velocity curve, it tends to be the most difficult parameter to obtain a reliable fit to, especially if there is insufficient phase coverage such as planets with periods longer than the observing window.

The iterative grid-search does have several features which should be noted. The grid precision essentially defines the resolution of the constructed grid. As such, one might naively expect that a linear increase in the grid precision will lead to a linear improvement in the fit of the model to the data. Although this generally tends to leads to a better χ^2 , the relationship is rather more complex and in fact one can

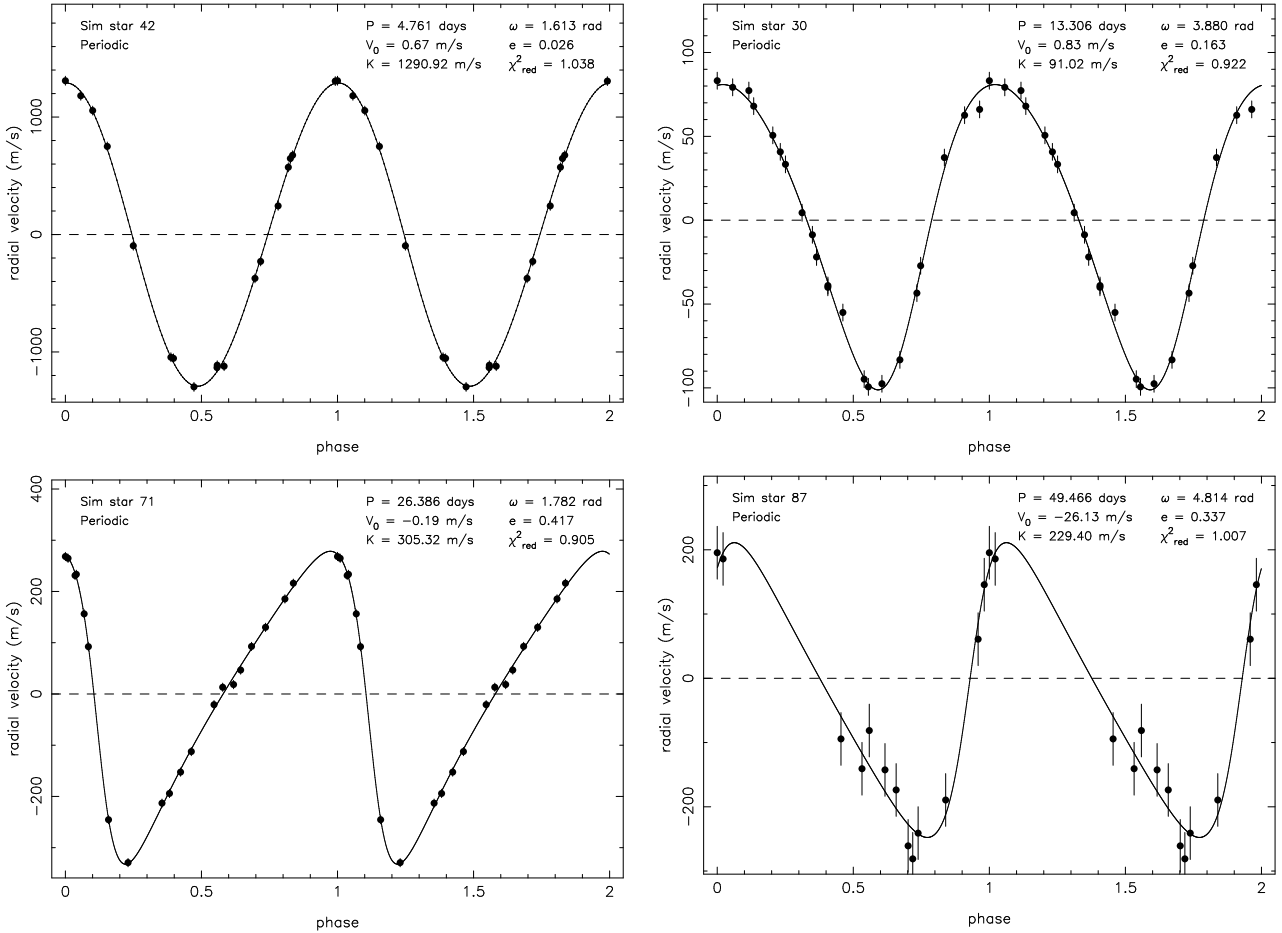


Figure 9. Examples of simulated radial velocity data for stars harbouring a planet and the best-fit models.

only be assured of an improved fit if the chosen g_p is twice the previous value, where the previous value is an even number. Even numbers tend to lead to better fits due to the way in which the grid is re-created on each iteration, meaning that the current best fit will be included as a grid-point in the refined grid. Since the number of model evaluations for a given iteration is equal to $(g_p + 1)^N$ where N is the number of fit parameters, the process can quickly becomes computationally expensive. It is therefore often the case that one uses a higher grid precision as a means of refining a fit at a later stage. Lastly, the fit relies quite heavily upon the initial guess of the planetary period and the mostly likely cause of a skewed fit is a relatively strong alias in the periodogram which has corrupted the fit. Provided one is able to recognise when this has occurred, it is quite straightforward to solve.

5.4 Uncertainties in Fit Parameters

The calculation of the uncertainties on each of the fit parameters is performed in a separate process to the model fitting described above. The uncertainties in the parameters are estimated using a Monte-Carlo simulation which passes the data through a gaussian filter based upon the error bars. Each successive dataset is then passed through the fitting

procedure resulting in an independent set of values for the fit parameters which are then stored in arrays. Repeating this operation a suitable number of times leads to a probability distribution of values for each parameter from which one can compute the sample variance to define the uncertainty in that parameter.

This is a powerful and robust method for defining the fit uncertainties but has certain drawbacks which should be mentioned. This method assumes that the uncertainties are gaussian in nature which is not always the case for ω and e . Indeed the probability distribution for ω is often double-peaked, which one can overcome by considering the two peaks as separate distributions. This method is also computationally expensive depending on how large a simulation is considered adequate to produce reliable statistics. However, since the uncertainties are calculated in a separate process to the overall fitting, this only need be performed when necessary.

6 TARGET SELECTION

Target selection is a crucial step to exclude giant stars and unstable stars from an exoplanet radial velocity survey. This is normally achieved through the use of catalogue information (such as that provided by Tycho-2 (Høg et al. 2000)

and 2MASS (Skrutskie et al. 2006)), reduced proper motion diagrams, and various other techniques. This process normally excludes the majority of stars in a given field as suitable targets since giant stars tend to be dominant in a magnitude-limited survey.

As a consequence of this, an important issue for multi-object surveys is having enough suitable targets within the given FOV. To investigate this aspect in detail, Besançon models for the COROT center ($l = 37.0^\circ; b = -6.9^\circ$) and anti-center ($l = 212.6^\circ; b = -1.1^\circ$) fields were constructed to compliment the existing Kepler field simulation. The benefits of choosing these fields are: (a) they are the subject of current and future searches for transiting exoplanets making them likely targets for complimentary radial velocity surveys, and (b) they represent diverse stellar densities due to their very different locations. The size of each of these fields was chosen to be 10 square degrees to provide a large enough sample, though the “eye” of COROT is significantly larger than this. For each of these fields, the giant stars were distinguished from the dwarf stars and a colour cutoff was imposed which excluded stars earlier than \sim F7.

Table 1 shows the results of this study which estimates the number of suitable targets per field. This was performed for a range of magnitude depths, with the bright end set to $V = 6$. An additional column was produced which scales the results to the size of the Sloan 2.5m FOV which is around 7 square degrees. These results are consistent with target number estimates from catalogue information, including the percentage rise in dwarf stars with increasing magnitude depth. This places fairly tight constraints on the number of planned fibres for a given instrument and magnitude depth, depending on the FOV. For example, the Keck ET instrument is currently able to monitor ~ 60 targets simultaneously (Ge et al. 2006), from which these conservative estimates show that there will be an adequate number of targets at a magnitude depth of $V = 12$ or fainter.

7 EXPECTED SURVEY RESULTS

The results one can expect from a given survey depends upon a number of factors, including the observing site, the efficiency of the instrument, and the number of stars observed. Here we estimate the overall survey results for our particular simulation and discuss how this can be translated into the expected number of planet discoveries from a particular experiment.

7.1 Total Planet Yield

The total number of planets in the simulated sample is ~ 750 . As shown in Figure 4, the number of planets undetectable due to the photon-limit of the survey is around 33% of this number, or 250 planets. This leaves ~ 500 planets remaining in the sample. The number of planets lost during the sifting of the data depends upon how strict a criteria is used to minimise the number of false detections. If we adopt a false-alarm probability threshold of 10%, thus producing essentially zero false detections, then Figure 7 shows that 45% of the remaining planets will be lost, or 225 planets. Thus, the number of planets detected in the survey is

around 37% of the total number of planets, or ~ 275 planets. Since there are around 25000 stars in the survey in this case, this means a detection rate of around 1% so that for every 100 stars surveyed, 1 star will have a planet that will be detected.

It must be remembered that this planet yield assumes a “blind” survey, meaning there are no other selection criteria for the stars included in the survey for the specified magnitude range other than to distinguish giant stars from dwarf stars. This can be improved upon using techniques discussed in later sections. It is a relatively straightforward calculation to scale this planet yield with the magnitude depth of the survey based upon the results shown in Table 1. In principle, each change in unit magnitude changes the volume of survey space and therefore the integrated star counts by a factor of ~ 4 . However, this is not true in practice due to interstellar absorption and the direction dependent spatial distribution of stars. For example, according to Table 1 the total number of stars in the Kepler field increases by a factor of ~ 2.5 per unit increase in magnitude depth for the range of magnitudes shown. For the COROT fields, this factor is closer to ~ 3.0 due to the proximity of these fields to the Galactic plane. The percentage number of dwarf stars increases with depth though and so the change in dwarf stars for each change in unit magnitude is ~ 3.5 . If, for example, the magnitude depth of the survey is decreased from 14 to 13, then the number of stars will decrease from 23708 to ~ 6800 and thus the number of detected planets will decrease to ~ 80 . Of course increasing the magnitude depth of the survey requires an equivalent improvement in radial velocity precision to prevent planetary signals becoming lost in the noise.

7.2 Survey Duration Dependence

If one increases the number of stars in the survey, then one can expect to increase the overall planet yield by a proportional amount. This is not the case for increasing the survey duration however since, although Figure 8 shows that successful detections for a given period increases linearly with the observing window, we have assumed a period distribution which is uniform in log space. Thus, the change in the number of planets to which one is sensitive can be determined by integrating over the region of the period distribution which matches the survey duration. For example, if the survey duration is increased to 60 days, then the number of additional planets N_a can then be approximately estimated as follows

$$N_a = \frac{N_p(60) - N_p(30)}{N_p(60)} N_t \quad (13)$$

where $N_p(30)$ and $N_p(60)$ are the number of planets with periods less than 30 days and 60 days respectively, and N_t is the total number of detected planets. For the simulation presented here, these numbers are 276, 344, and 275 respectively, resulting in an additional 67 possible planet detections at larger periods. As mentioned in section 3.4, this assumes that the planet distribution only includes one planet per planet-harbouring star. The fractional number of multiple exoplanetary systems is currently known to be ~ 0.12 . Thus we can also estimate the number of additional planets in longer orbits N_m for those systems already detected

Table 1. Number of dwarf stars available based on Besancon models of the Kepler field, COROT center field, and COROT anti-center field.

Field	V mag	stars	giants	dwarfs	% dwarfs	dwarfs	\square°	Sloan	FOV
Kepler	< 14	62114	43746	18368	29.6	174		1218	
	< 13	25942	20843	5099	19.7	48		336	
	< 12	10117	8701	1416	14.0	13		91	
COROT center	< 14	15289	13017	2272	14.7	227		1589	
	< 13	4803	4207	596	12.4	59		413	
	< 12	1439	1298	141	9.8	14		98	
COROT anti-center	< 14	6570	4833	1737	26.4	173		1211	
	< 13	2284	1821	463	20.3	46		322	
	< 12	847	720	127	15.0	12		84	

$$N_m = 0.12(N_t + N_a) \quad (14)$$

leading to 41 additional planets in multiple-planet systems. This assumes that the survey duration has been sufficiently extended to be sensitive to the outer planets and that the observing strategy allows for continued monitoring of those stars. This is of course a rough estimate, but is sufficient as a lower limit as it is expected that the known fractional number of multiple exoplanetary systems will only increase with time. It is also likely that these systems will contain planets with longer periods that can be discovered through continued monitoring.

7.3 Eccentricity Bias

The chosen observing schedule undoubtedly influences the sensitivity to various planetary orbital parameters. Perhaps the most significant effect on the detection efficiency is due to the eccentricity of the planet. Highly eccentric orbits exhibit a rapid change in radial velocity which is likely to result in a failure of their periodic detection via Fourier analysis if there are reasonably large gaps in the observing schedule. Since most of the observations will occur when the planet is closest to apastron when the radial velocity changes are at their lowest, the overall effect in terms of the detection will be similar to that of planets whose period is much large than the duration of the survey as discussed earlier. The highly eccentric planets can still be detected if their apastron radial velocity variations exceed that required by the variability test, such as the one discussed in section 5.1. This will be true in most cases.

To provide a quantitative estimate of the bias against detecting eccentric planets, a simulation was constructed identical to the one described in section 4 except for the following: (1) the eccentricity was uniformly distributed between 0 and 1 and (2) the 30 days of observations were split into three groups of 10 consecutive days with each group separated by 20 days. This observing strategy is quite typical of experiments which have only intermittent access to telescope time. This configuration was used to simulate over 4.7×10^6 planet-harbouring datasets which were passed through the sifting algorithm described in section 5.1 and using a strict false-alarm probability threshold to eliminate false detections.

The results of this exhaustive simulation are shown in Figure 10. The detection efficiency begins to become severely affected for planets with eccentricities greater than ~ 0.6 , as shown by the solid line which represents datasets flagged as periodic by the Fourier analysis. If one includes the planets

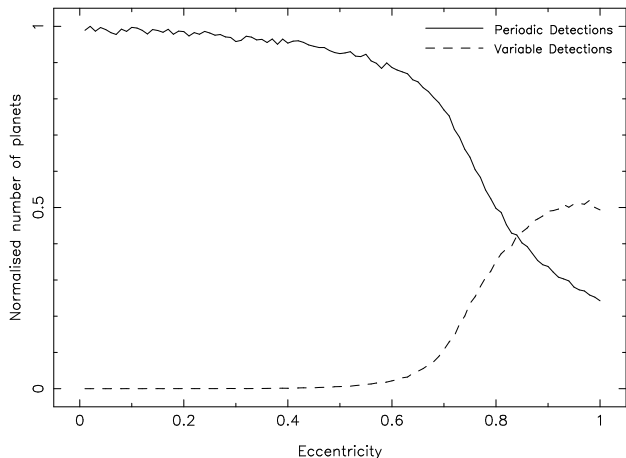


Figure 10. The effect of planetary eccentricity on the planet detection efficiency for an observing schedule which utilises a 10 consecutive nights for 3 months strategy.

which have been flagged as having an rms scatter significantly greater than the standard deviation of the data, then one is able to recover many of the highly eccentric planets despite the lack of phase coverage. This is an expected result but worth highlighting in a qualitative fashion in order that surveys can judge their bias against the eccentric planets when planning the observing strategy.

7.4 Total Transiting Planets

The popularity of the transit method to detect extra-solar planets is self-evident by the large number of independent teams currently using the technique for planet hunting. The reason that the transit method has become so popular is due to the radial velocity surveys discovering a relatively high number of “hot Jupiters” orbiting solar-type stars. In fact, 0.5%–1% of Sun-like stars in the solar neighbourhood have been found to harbour a Jupiter-mass companion in a 0.05 AU (3–5 day) orbit (Lineweaver & Grether 2003). The probability, P_t , of a planet producing an observable transit can be described by

$$P_t = \frac{(R_\star + R_p)}{a} \approx \frac{R_\star}{a} \quad (15)$$

where R_\star and R_p are the radii of the star and planet respectively. It is reasonable to assume that the orbital plane of these short-period planets are randomly oriented, which according to the geometric transit probability means that approximately 10% of these planets will transit the face of

their parent star as seen by an observer. Thus, the transit method is favoured considering the conclusion that close to 1 in 1000 solar-type stars will produce detectable transits due to an extra-solar planet. Since this transit method clearly favours large planets orbiting their parent stars at small orbital radii, many of the hot Jupiters discovered via radial velocity surveys are expected to also exhibit a photometric transit signature.

To approximate the number of transiting planets expected from the simulated survey, the geometric transit probability was calculated for each star/planet system as part of the Monte-Carlo simulation discussed in section 3.4. In each case, it was randomly determined if the planet does indeed transit the parent star. For the 751 planets contained in the simulation, it was consistently found that 30 observable transiting planets can be expected to be present. This estimation takes into account the entire period range which is why it is significantly smaller than 10% of the total planet population. It is assumed that we will only detect transiting planets as a result of photometrically monitoring the detected planets with shorter periods, and hence the total number of detected transiting planets will be a factor of 37% smaller, as per section 5.1, or 11 transiting planets. Observing strategies for optimal photometric detection of the transiting planets from radial velocity surveys are discussed elsewhere (Kane 2007).

8 DISCUSSION

One of the main goals of this paper has been to approximate the expected number of planets from a large scale radial velocity survey. There are limitations to the simulation which should be noted, however. Section 3.4 describes the method used to create a realistic distribution of planet parameters from which the characteristics of each planet was drawn from. Great effort has been made to ensure that these parameter distributions are as free from bias as possible. One of the most obvious cases where bias is possible to have crept in is the period distribution. The period range was chosen to ensure that as many stars as possible will have been monitored for at least as long as the upper end of the chosen range. In addition, transiting planets were excluded due to their obvious bias towards shorter periods. Even so, any unaccounted for bias towards shorter periods will lead to an over-estimation in the number of planets detected depending on the survey duration.

The method used for fitting the radial velocity data in this paper is described as an iterative grid-search method. There are certainly other methods used elsewhere for which a comparison would prove useful. A powerful method used in a wide variety of astronomical applications is the method of Bayesian analysis. Bayesian analysis is a statistical procedure which uses a prior distribution of the parameter values in combination with the observed distribution to create a probability map over all possible values. Thus Bayesian methods deliver not only the the optimal parameter values but also their complete joint posterior probability distribution which also determines the uncertainties in the parameters. This method has been used successfully for extracting periodic exoplanet signatures in radial velocity data (Ford 2006; Gregory 2005). Another common data-fitting method

is the use of genetic algorithm (Charbonneau 1995). Like simulated annealing, this method is specifically designed to overcome the difficult problem of avoiding local minima in χ^2 space by allowing individual groups of fits to develop in a manner similar to evolutionary biology where the best traits of each fit are passed on to the next generation. The main purpose of the current sifting and fitting code is to flag those data for which periodic signals are suspected to be present from which any optimal fitting method can then be adopted.

The Besançon model provides a very effective and convenient method to aid in selecting optimal fields in which to conduct a particular survey. As mentioned earlier, this approach was used by Jenkins et al. (2005) to choose the best field for the upcoming Kepler mission. In particular, both transit and radial velocity surveys are concerned with the number of giant stars in the survey fields as substantial numbers of these stellar types can drastically reduce the expected planet yield. Creating comparative Besançon models for a selection of proposed field centers can thus be used in combination with typical methods for sifting dwarf stars, such as reduced proper motion diagrams, to provide optimal target selection for the survey.

An aspect which is not considered in the simulation is the inclusion of high-mass stars in the sample, since most surveys to date have focused their attention on F–G–K stars. It has been noted, for example by Galland et al. (2005), that high-precision radial velocity measurements of early A–F stars is exceptionally difficult, mostly due to the lack of spectral lines usable for cross-correlation and the line-broadening caused by high rotational velocities. For this reason, one may decide that early-type stars are inaccessible to the survey in question. However, the results of the simulation are not substantially changed if high-mass are excluded since they only contribute a small percentage to the total number of stars.

The Besançon model for the Kepler fields predicts a metallicity distribution which increases towards sub-solar metallicity. This low metallicity bias is not an unexpected result, since the metal-poor nature of the field stars will always be true to varying degrees for a magnitude-limited survey which essentially only probes the solar neighbourhood. Surveys such as that performed by the N2K consortium (Robinson et al. 2006) estimate atmospheric parameters via low-resolution spectroscopy to screen low-metallicity stars from their survey targets. The survey proposed using the Keck ET instrument will be able to screen giant stars and, in a more limited capacity, active stars via photometry available from photometric catalogues, but is otherwise a “blind” survey in many regards. The survey is more than able to compensate for this simply due to the vast amount of stars one is able to survey thanks to the multi-object capabilities of the instrument. Hence, with an equivalent radial velocity precision, one expects that N2K will detect a higher rate of planets per survey star, but the Keck ET survey will detect a much higher overall number of planets.

9 CONCLUSIONS

With the introduction of multi-object spectrographs capable of high-precision measurements, the rate of planet detection is expected to rise significantly. This paper presents

simulations of a sample of stars from the Kepler field which demonstrate the advantages of using such an instrument and a rough guide on how many planets could be expected to be detected given a certain noise model and magnitude limit.

The simulated data was derived from a Besançon model of the Kepler field which is an ideal location to perform a radial velocity survey complimentary to planned future transit surveys. The stellar metallicities from the model allowed the estimation of planet frequency based on a Monte-Carlo simulation which utilises the well-known planet-metallicity correlation. This produced 751 planets from 23708 stars with a cumulative histogram which shows the rapid decline in planet-harbouring stars beyond a probability of around 5%. The distribution of planetary parameters were derived from a numbers of sources to produce as accurate a representation as possible of the expected planets in the simulation.

The noise model and the simulated planets were the subject of an additional Monte-Carlo simulation which demonstrated the number of planet detections one can expect from a given radial velocity precision. This showed that, in general, doubling the number of stars will increase the number of planets a factor of five more than doubling the precision of the instrument. The number of targets is thus by far the dominant factor in a survey, hence the advantage of multi-object instruments is clear.

When the number of targets is increased significantly, the sifting of the data for planetary signatures becomes an important process in order to reduce the number of false detections and increase the number of real detections in a manner which is not too computationally expensive. By using a weighted Lomb-Scargle fourier analysis in combination with variability statistics, it is shown that only a slight reduction in the number of real detections leads to a complete elimination of false detections. Also, it is shown that at least 15 data points is generally needed for a significant detection. The number of these detections decreases linearly with the fractional period as compared to the observing window.

The results from the simulation showed that around 37% of the total number of planets in the survey could be feasably detected, leading to around 1 detected planet for every 100 stars surveyed. This is dependant upon the magnitude limit of the survey and the survey duration, an increase of which will lead to not only longer period planets, but also multiple planetary systems. The number of transiting planets was calculated from the geometric transit probability and was found to be around 11 transiting planets over the entire period range. This simulation was designed based upon the current survey being performed using the Keck ET instrument, however these planet yields can be quite easily scaled to take into account the specifics of any particular planet survey.

Since most multi-object surveys are most sensitive to Jovian planets with periods less than around 5 days, the total planet yield is quite sensitive to the chosen period distribution. As the duration of existing surveys increase, an unbiased knowledge of the period distribution will improve and will lead to more accurate simulations. With many space missions, such as Kepler, which are expected to discover many hundreds of extra-solar planets in the near future, multi-object radial velocity surveys will provide invaluable complimentary orbital parameters for these systems.

ACKNOWLEDGEMENTS

The authors would like to thank Suvrath Mahadevan, Eric Ford, Curtis DeWitt, and Roger Cohen for several useful discussions. This work is supported by the W.M. Keck Foundation, the University of Florida, and National Science Foundation grant AST-0451407.

REFERENCES

Adams, F.C., Laughlin, G., 2006, *ApJ*, 649, 992
 Adams, F.C., Proszkow, E.M., Fatuzzo, M., Myers, P.C., 2006, *ApJ*, 641, 504
 Aharmin, B., et al., 2005, *Phys. Rev. D*, 72, 052010
 Beaulieu, J.P., et al., 2006, *Nature*, 439, 437
 Borucki, W.J., et al., 2003, *ASP Conf. Series*, Vol. 294, *Scientific Frontiers in Research on Extrasolar Planets*, eds. D. Deming & S. Seager, p. 427
 Bouchy, F., Pepe, F., Queloz, D., 2001, *A&A*, 374, 733
 Bouchy, F., Pont, F., Santos, N.C., Melo, C., Mayor, M., Queloz, D., Udry, S., 2004, *A&A*, 421, L13
 Bouchy, F., Bazot, M., Santos, N.C., Vauclair, S., Sosnowska, D., 2005, *A&A*, 440, 609
 Butler, R.P., Marcy, G.W., Williams, E., McCarthy, C., Vogt, S.S., 1996, *PASP*, 108, 500
 Butler, R.P., et al., 2006, *ApJ*, 646, 505
 Charbonneau, P., 1995, *ApJS*, 101, 309
 Charles, E.D., Tatum, J.B., 1998, *CeMDA*, 69, 357
 Dall, T.H., Santos, N.C., Arentoft, T., Bedding, T.R., Kjeldsen, H., 2006, *A&A*, 410, 983
 Deming, D., Harrington, J., Seager, S., Richardson, L.J., 2006, *ApJ*, 644, 560
 Fischer, D.A., et al., 2005, *ApJ*, 620, 481
 Fischer, D.A., Valenti, J., 2005, *ApJ*, 622, 1102
 Ford, E.B., 2006, *ApJ*, 642, 505
 Galland, F., Lagrange, A.-M., Udry, S., Chelli, A., Pepe, F., Queloz, D., Beuzit, J.-L., Mayor, M., 2005, *A&A*, 443, 337
 Ge, J., 2002, *ApJ*, 571, L165
 Ge, J., et al., 2006, *ApJ*, 648, 683
 Ge, J., et al., 2006, *Proc. SPIE*, 6269, 75
 Gregory, P.C., 2005, *ApJ*, 631, 1198
 Gunn, J.E., et al., 2006, *AJ*, 131, 2332
 Høg, E., et al., 2000, *A&A*, 355, L27
 Horne, K., 2003, *ASP Conf. Series*, Vol. 294, *Scientific Frontiers in Research on Extrasolar Planets*, eds. D. Deming & S. Seager, p. 361
 Jenkins, J.M., Chandrasekaran, H., Caldwell, D.A., Batalha, N.M., Silva, N., Koch, D.G., Gautier, T.N., 2005, *DPS*, 37, 31.08
 Jorissen, A., Mayor, M., Udry, S., 2001, *A&A*, 379, 992
 Kane, S.R., Collier Cameron, A., Horne, K., James, D., Lister, T.A., Pollacco, D.L., Street, R.A., Tsapras, Y., 2005, *MNRAS*, 364, 1091
 Kane, S.R., 2007, *MNRAS*, submitted
 Lee, M.H., Peale, S.J., 2002, *ApJ*, 567, 596
 Lin, D.N.C., Bodenheimer, P., Richardson, D.C., 1996, *Nature*, 380, 606
 Lineweaver, C.H., Grether, D., 2003, *ApJ*, 598, 1350
 Lomb, N.R., 1976, *Ap&SS*, 39, 447
 Marcy, G.W., Butler, R.P., Williams, E., Bildsten, L., Graham, J.R., Ghez, A.M., Jernigan, G., 1996, *ApJ*, 481, 926

Marcy, G., Butler, R.P., Fischer, D., Vogt, S., Wright, J.T.,
Tinney, C.G., Jones, H.R.A., 2005, PThPS, 158, 24

Mahadevan, S., Ge, J., van Eyken, J., Cohen, R., DeWitt,
C., Wan, X., 2005, Protostars and Planets V Proceedings,
Contribution No. 1286., p. 8224

Mosser, B., et al., 2005, A&A, 431, L13

Pasquini, L., et al., 2002, The Messenger, 110, 1

Pepe, F., et al., 2004, A&A, 423, 385

Rasio, F.A., Ford, E.B., 1996, Science, 274, 954

Robin, A.C., Reylé, C., Derrière, S., Picaud, S., 2003, A&A,
409, 523

Robinson, S.E., Strader, J., Ammons, S.M., Laughlin, G.,
Fischer, D., 2006, ApJ, 637, 1102

Saar, S.H., Butler, R.P., Marcy, G.W., 1998, ApJ, 498,
L153

Saar, S.H., Fischer, D., 2000, ApJ, 534, L105

Santos, N.C., et al., 2004, A&A, 426, L19

Scargle, J.D., 1982, ApJ, 263, 835

Skrutskie, M.F., et al., 2006, AJ, 131, 1163

Szentgyorgyi, A.H., Cheimets, P., Eng, R., Fabricant, D.G.,
Geary, J.C., Hartmann, L., Pieri, M.R., Roll, J.B., 1998,
Proc. SPIE, 3355, 242

Tabachnik, S., Tremaine, S., 2002, MNRAS, 335, 151

Udry, S., et al. 2003, A&A, 407, 679

van Eyken, J.C., Ge, J., Mahadevan, S., DeWitt, C., 2004,
ApJ, 600, L79

Wright, J.T., 2005, PASP, 117, 657

Zucker, S., Mazeh, T., 2001, ApJ, 562, 1038